RSC Advances

ROYAL SOCIETY OF CHEMISTRY

www.rsc.org/advances

Graphical and textual abstract

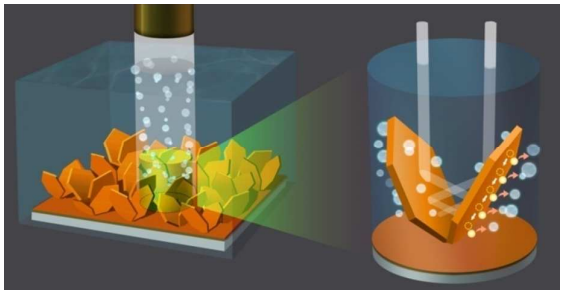

We present a scalable route for the preparation of single crystalline Cu_2ZnSnS_4 nanosheet arrays on conductive glass substrate, and demonstrate this architecture as an effective photocathode for solar hydrogen production.

RSC Advances

RSCPublishing

ARTICLE

Single Crystalline Cu_2ZnSnS_4 Nanosheet Arrays for Efficient Photochemical Hydrogen Generation

Cite this: DOI: 10.1039/x0xx00000x

Bo-Jun Li,† Peng-Fei Yin,† Yu-Zhu Zhou, Zhi-Ming Gao, Tao Ling,* Xi-Wen Du*

Received ooth January 2012,
Accepted ooth January 2012

DOI: 10.1039/x0xx00000x

www.rsc.org/

Cu_2ZnSnS_4 (CZTS) is promising for application in photoelectrochemical (PEC) water splitting system, owing to its high absorption coefficient, abundance, non-toxicity and direct band gap suitable for solar conversion. Here we present a scalable route for the preparation of single crystalline CZTS nanosheet arrays (NSAs) on conductive glass substrate by using CuS nanosheets (NSs) as a sacrifice template. When employed as a photocathode for PEC solar hydrogen production, the CZTS NSAs yield a photocurrent density of -1.32 mA/cm^2 at 0 V versus the reversible hydrogen electrode under illumination of AM 1.5. This is the highest value ever reported for CZTS-based electrode without co-catalyst and protective layer. The CZTS NSAs photocathode remains active after 3.5 h testing and maintains 60% of its initial photocurrent. This work demonstrates the reality of using earth-abundant CZTS for efficient hydrogen production.

1. Introduction

Photoelectrochemical (PEC) splitting of water under sunlight is attractive and efficient for the generation of clean hydrogen, which represents a promising solution to the energy crisis and global warming in the future.[1-5] Since the pioneering work by Honda and Fujishima,[6] extensive efforts have been directed to exploring inexpensive and stable semiconductor materials as efficient photoelectrodes in the PEC water splitting system.[4,7-9] Cu_2ZnSnS_4 (CZTS), a p-type semiconductor, has attracted much attention due to its high absorption (>10^4 cm^{-1}), abundance, non-toxicity and direct band gap (E_g=1.5 eV) suitable for solar energy conversion.[10,11] For PEC water splitting, CZTS possesses a theoretical photocurrent of 25 mA/cm^2 under the AM 1.5 irradiation,[12] thus being highly expected to function as an efficient photoelectrode.

Recently, CZTS has been experimentally explored in PEC water splitting system.[13-18] Domen *et al.* firstly reported the PEC properties of modified CZTS film in 2010.[13] Zou *et al.* fabricated porous CZTS film and gained a photocurrent of about 0.4 mA/cm^2 at a potential of 0 V versus the reversible hydrogen electrode (RHE).[14] More recently, Sivula *et al.* protected CZTS film by sequentially depositing CdS/AZO/TiO_2/Pt layers, and obtained a photocurrent over 1 mA/cm^2 (at 0 V versus RHE) under standard one sun illumination.[15] Collectively, the conversion efficiencies of CZTS photocathodes are still far below the theoretical value due to the poor crystal quality of the nanocrystalline CZTS film, which results in short lifetime of minority carriers.[14] Moreover, the minus carrier diffusion length (several hundred nanometers) is much smaller than the light absorption depth near the band gap (approximately 2 μm),[19] leading to insufficient extraction of carriers and lower water splitting efficiency.[20]

The disadvantages of nanocrystalline CZTS film may be overcome by engineering high quality three-dimentional (3D) nanostructures. Herein, we suggest a model structure of single crystalline nanosheet arrays (NSAs). As shown in Scheme 1, the single crystalline nanosheets (NSs) demonstrate several unique advantages. First, they offer direct electrical pathways for photo-generated carriers, which remarkably increase the collection efficiency of majority carriers.[21-23] Second, the NSs possess large surface area, which increases the reaction area and improves the surface evolution kinetics. Third, the small thickness of NSs can reduce the diffuse length of minority carriers significantly, which improves their utility.[24-26] Fourth, the NSAs enhance light absorption by effective light scattering and trapping.[25,26] All the above can enhance carrier lifetime and PEC activity. Hence, such architecture is promising for CZTS application in PEC solar hydrogen production.

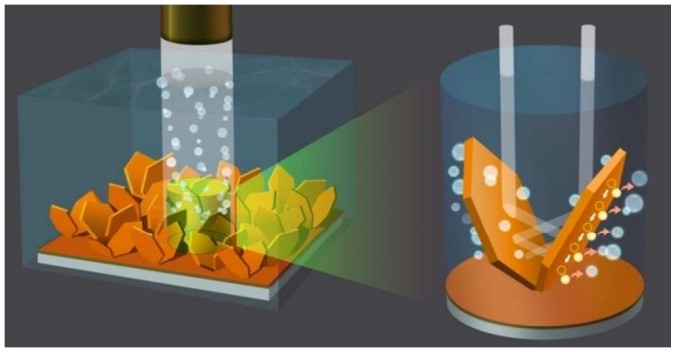

Scheme 1 Schematic illustration of (a) single crystalline CZTS NSAs generating hydrogen under illumination, and (b) light scattering, charge separation and transportation in NSs.

To test the above hypothesis, we developed a scalable template method to fabricate single crystalline CZTS NSAs directly on transparent conductive substrate. We found the CZTS NSAs could trap incoming light effectively, present superior conductivity, and possesses favorable energy bands for water splitting. When being employed as photocathode in water splitting system, CZTS NSAs achieved a photocurrent up to -1.3 mA/cm^2 at a potential of 0 V versus RHE under AM 1.5 solar illumination. This is the highest value ever reported for CZTS photocathodes without cocatalyst and surface modification.

2. Experimental

2.1 Preparation of CuS NSAs

Firstly, CuCl film was grown on a FTO substrate by vacuum evaporation deposition. Specifically, 0.03 g CuCl was placed in the middle of the tube furnace, and a cleaned FTO was located about 40 cm away from the center with the conductive side upward. Then the tube was evacuated to -100 kPa, maintained at 400^{o}C for 30 min. Secondly, CuCl film was sulfurized to fabricate CuS NSAs. The FTO substrate covered with CuCl film and sulfur powder were put together into a graphite boat. Then, the tube was evacuated to -100 kPa and heated to 285^{o}C. Subsequently, the graphite boat was inserted into the center of the furnace. The temperature was kept at 285^{o}C for 40 min, and finally, the furnace was cooled down under vacuum to room temperature.

2.2 Preparation of CZTS NSAs

The CZTS NSAs were obtained by a solvothermal process. 70 mg $Zn(CH_3COO)_2{\cdot}2H_2O$ and 70 mg $SnCl_2{\cdot}2H_2O$ were dissolved in 40ml triethylene glycol, and then transferred to a Teflon-lined stainless steel autoclave. CuS NSAs covered FTO substrate was dipped into the autoclave vertically. The autoclave was sealed and maintained at 205^{o}C for 40 h, and naturally cooled to room temperature. CZTS NSAs were washed with distilled water and dried in vacuum at 60^{o}C.

2.3 Preparation of CZTS film

The CZTS film was synthesized via solution phase method according to the literature.[27] Firstly, the precursor solution was prepared by dissolving 0.8 mmol $Cu(CH_3COO)_2{\cdot}2H_2O$, 0.56 mmol $ZnCl_2$, 0.55 mmol $SnCl_2{\cdot}2H_2O$ and 2.64 mmol thiourea into 0.7 ml dimethyl sulfoxide while stirring at room temperature. Secondly, the precursor solution was spin coated onto a FTO substrate at 1500 rpm for 1 min and followed by annealing in N_2 atmosphere at 420^{o}C for 20 min. This coating step was repeated six times to obtain CZTS film with proper thickness.

2.4 Photoelectrochemical measurements

The PEC measurements were recorded by using Versastat 3 Potentiostats Electrochemistry workstation. A three-electrode configuration was adopted where Ag/AgCl in saturated KCl (0.197 V versus normal hydrogen electrode, NHE) and Pt foil were used as reference and counter electrodes, respectively. The electrolyte was a solution of 0.3 M Na_2SO_4 with the pH adjusted to about 9.5 using 1 M NaOH solution. The current density-potential curves were measured in dark and under irradiation from a 300 W Xe lamp, calibrated with a standard Si solar cell to simulate AM 1.5 illumination (100 mWcm^{-2}). The scan rate for the linear sweep voltammetry was 5 mVs^{-1}. Photocurrent stability test was carried out by measuring the photocurrent produced under constant light irradiation at a fixed electrode potential of 0 V versus RHE.

2.4 Characterization

Crystallographic information on the CuS and CZTS structures was studied with Bruker-D8 XRD. Dimensions, morphologies, crystal lattices, and composition of the samples were characterized with SEM (Hitachi S-4800), TEM and SAED (Technai G2 F20 with a field emission gun operated at 200 kV). The composition was analyzed by an EDS module attached on TEM. AFM (Agilent 5500) was applied to determine the thickness of the CZTS NS. Optical absorption data were recorded with a Hitachi UV4100. Raman spectra were measured with a Renishaw 2000 system with a 532 nm excitation source. XPS spectra were carried out with PHI-1600 ESCA spectrometer analysis system with a monochromatic Al Kα X-ray source (1486.6 eV). The Mott-Schottky curves were measured using an electrochemical analyser (Princeton Applied Research, 2273).The electrolyte was 0.3 M Na_2SO_4 aqueous solution (pH was adjusted to 9.5). The ac amplitude was 10 mV and the frequency was 1000 Hz. The atomic absorption analysis was performed with WFX-130 AAS. EIS data were collected by using a Versastat 3 Potentiostats Electrochemistry workstation in the frequency range from 0.1 Hz to 100 kHz at open-circuit conditions.

2.5 FDTD Simulation

All the simulations were carried out by using commercial software named FDTD solution. The values of wavelength-dependent refractive indices and extinction coefficients for CZTS were extracted from the literatures.[28] Time step for every calculation is 0.02 fs. 2-D models of two samples are shown in supporting information. Boundary condition in X direction is periodic, while in Y direction is perfectly matched layer.

3. Results and Discussion

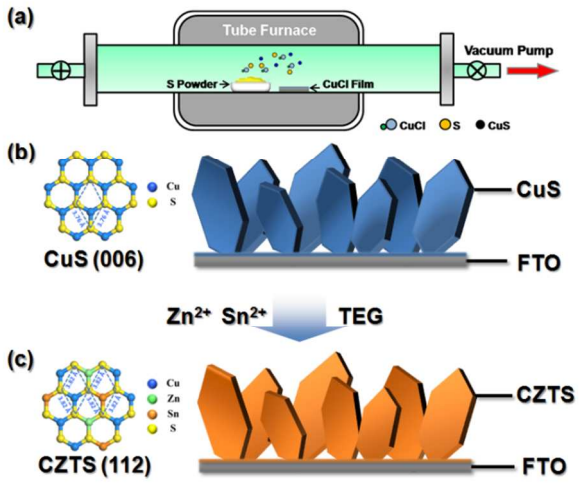

Scheme 2 Schematic illustration of the synthesis strategy of CZTS NSAs. (a) Experimental setup for synthesis of single crystalline CuS NSAs. (b) to (c) is transformation of CuS NSAs to Cu_2ZnSnS_4 (CZTS) NSAs, and the left side of panel (b) and (c) are S atomic arrangements in (006) plane of CuS and (112) plane of CZTS, respectively.

The synthetic process is shown in Scheme 2. First, CuCl film was deposited onto a conductive substrate via thermal evaporation (Supporting Information, Fig. S1). Second, the CuCl film was sulfurized to produce single crystalline CuS NSAs (Scheme 2a). Third, CuS NSAs were converted to CZTS counterparts by solvothermal reaction in a teflon-lined stainless steel auto clave containing Zn^{2+}, Sn^{2+} and reducing agent triethylene glycol (TEG) (Scheme 2b to 2c).

Fig. 1a presents a top-view scanning electron microscope (SEM) image of CuS NSAs, showing partially overlapped polygons with smooth edges and diameter about 3 to 5 microns. The side-view SEM image (Fig. 1b) illustrates that CuS NSs are in direct contact with the substrate. The phase composition was determined by X-ray diffraction (XRD) analysis (Fig. 1c). All the peaks can be indexed well to those of hexagonal covellite structure of CuS (JCPDS No. 06-0464). The transmission electron microscope (TEM) image shown in Fig. 1d exhibits a well-defined shape of as-synthesized CuS NS. The selected area electron diffraction (SAED) pattern of the CuS NS (Fig. 1e) can be indexed to the [001] zone axis of hexagonal CuS, indicating that the CuS NS possesses a single crystal structure and an exposed (001) face. The high-resolution TEM (HRTEM) image (Fig. 1f) clearly illuminates highly crystalline NS, where the lattice spacing of 0.33 nm corresponds to the (100) plane of CuS. The energy-dispersive X-ray spectroscopy (EDS) result demonstrates the presence of Cu and S elements with atomic ratios close to the stoichiometry of CuS (Supporting Information, Fig. S2).

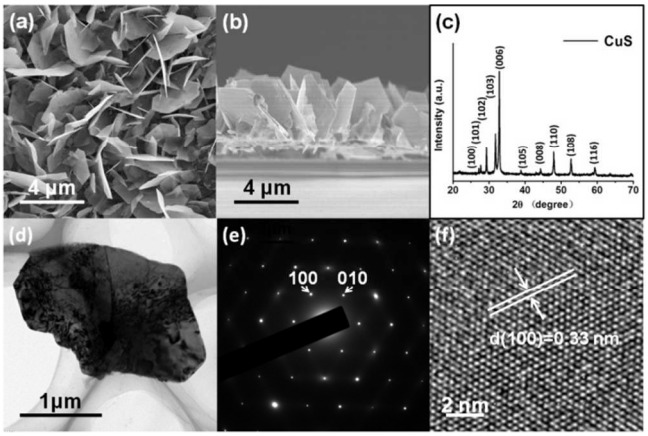

Fig. 1 Characterizations of CuS NSAs. (a) and (b) are top-view and side-view SEM images of CuS NSAs on a conductive glass substrate, respectively. (c) XRD pattern of the as-synthesized CuS NSAs. (d)-(f) are TEM image, SAED pattern and HRTEM image of a CuS NS, respectively.

The as-synthesized CuS NSAs were converted to CZTS NSAs via polyol reduction reported in literature.[29] The sheet shape of CZTS NSs in Fig. 2a and 2b kept intact after the solvothermal reaction. The cross-sectional height profile (Fig. 2c, bottom) shows that the NS thickness is approximately 35 nm, accordingly, the specific surface area of CZTS NSs was estimated to be 22.6 m^2/g (see details in part 4 of Supporting Information). The crystal structure of as-synthesized CZTS NSs was further examined by XRD and TEM. The XRD diffraction peaks (Fig. 2d) are all attributed to tetragonal CZTS (JCPDS No. 26-0575). The SAED pattern (Fig. 2e, inset) taken from a whole NS presents only one set of diffraction spots, confirming that the as-synthesized CZTS NS possesses a single crystal structure. This SAED pattern is indexed to a tetragonal structure with a zone axis of [221], suggesting an exposed (112) surface of CZTS. As seen in Scheme S1, the lattice of CZTS matches well with that of CuS, also, the S atomic arrangements in (112) plane of CZTS is similar with that in (006) plane of CuS (Supporting Information), the two factors facilitate the conversion of CuS to CZTS. Moreover, forbidden spots of $1/3\times(\bar{4}24)$ and $2/3\times(\bar{4}24)$ planes are observed due to stacking faults in the tetragonal structure.[30] The weaker spots $(10\bar{2})$ and $(1\bar{1}0)$ marked by white arrows are kinetically forbidden, indicating some disordering exists in the cation lattice.[30] The HRTEM image (Fig. 2f) shows lattice fringes with a spacing of d= 0.19 nm, which corresponds to the $(\bar{2}20)$, $(0\bar{2}4)$ and $(\bar{2}04)$ lattice planes of the tetragonal CZTS structure. The elemental mapping images (Supporting Information, Fig. S3) show homogenous distribution of Cu, Zn, Sn and S elements in the NS, and the relative elemental ratio of Cu:Zn:Sn:S is determined as 2.0: 1.0: 1.0: 3.9, agreeing well with its stoichiometric ratio. X-ray photoelectron spectroscopy (XPS) analysis was performed to investigate the oxidation states of NS surface (Fig. 3). Two peaks located at 952.2 and 932.2 eV confirm the existence of Cu^+ (Fig. 3a). The Zn 2p peaks at 1045.3 and 1022.3 eV suggest the presence of Zn^{2+} (Fig. 3b). Sn^{4+} state is identified from the core level peaks at 495.4 and 486.9 eV (Fig. 3c).The two peaks centred at 162.8 and161.7 eV (Fig. 3d) are assigned to $2p_{3/2}$ and $2p_{1/2}$ of sulfur.[31]

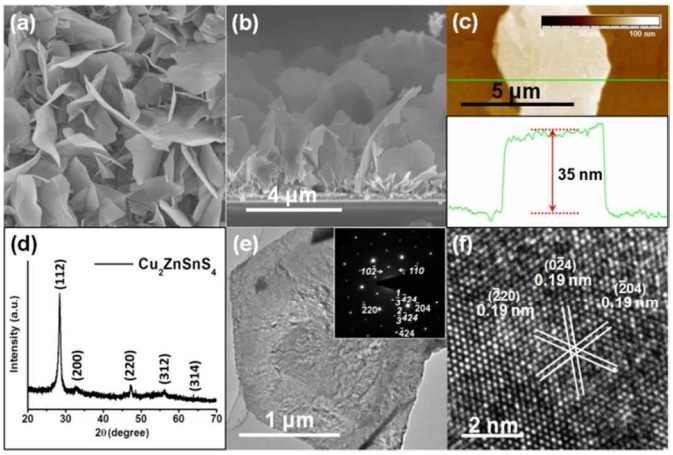

Fig. 2 Characterization of CZTS NSAs. (a) and (b) are top-view and side-view SEM images of CZTS NSAs on a conductive glass substrate, respectively.(c) AFM image of a single CZTS NS (top) and line-scan profile (bottom). (d) XRD spectrum of the as-synthesized CZTS NSs. (e) and (f) are TEM image and HRTEM image of the CZTS NS, respectively, and the inset of (e) is the SAED pattern of the NS shown in (e).

Further structural homogeneity of as-synthesized CZTS NSs was examined by Raman spectrum (Supporting Information, Fig. S4). The characteristic Raman peak at 332 cm^{-1} matches well with lattice vibration of bulk CZTS.[32] It is worth noticing that there are no additional peaks corresponding to other phases, such as CuS, ZnS and SnS, coinciding with XRD result (Fig. 2d). The corresponding band gap of CZTS was obtained as 1.43 eV (Supporting Information, Fig. S5), consistent with the values reported in the literature.[23]

Based on XRD, SAED, HRTEM, EDS, XPS and Raman characterizations, it is collectively concluded that single

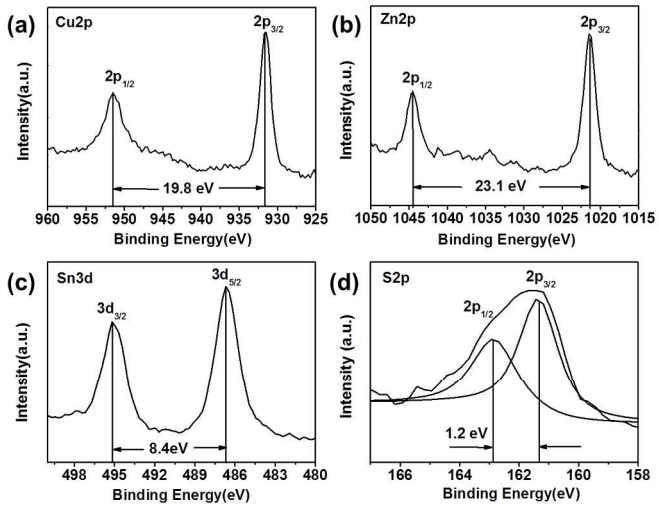

Fig. 3 High-resolution XPS analysis of CZTS NSs. (a)-(d) are the signals of Cu 2p, Zn 2p, Sn 3d and S 2p, respectively.

crystalline CZTS NSs were successfully fabricated. It should be noted that this is the first report on fabrication CZTS nanostructure directly on conductive glass substrate,[23] which is of crucial importance for optoelectronic devices.

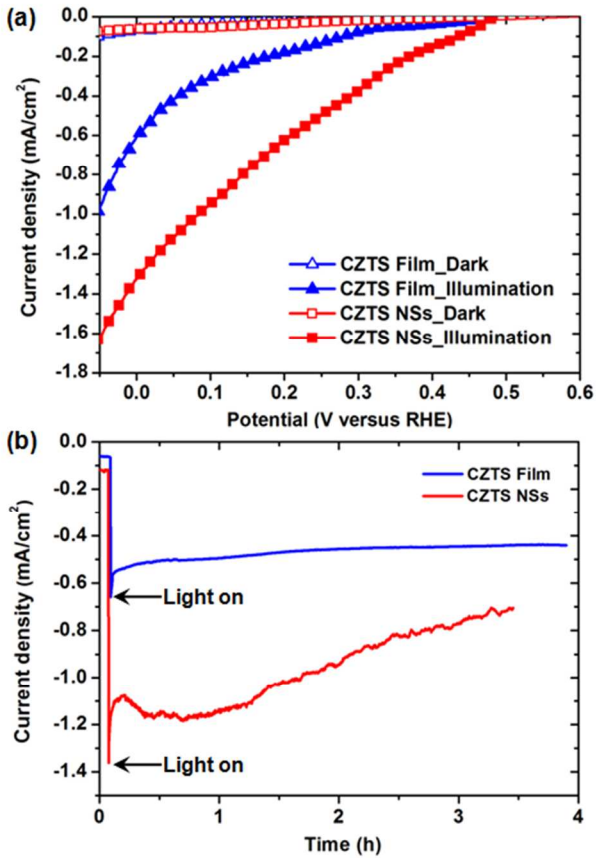

Fig. 4 Photoelectrochemical response of CZTS photocathodes. (a) The current density-potential plots of CZTS photocathodes in dark and under AM 1.5 light illumination in 0.5 M Na_2SO_4 solution (pH 9.5). (b) Stability of CZTS photocathodes at 0 V versus RHE under AM 1.5 illumination.

As-synthesized CZTS NSs were employed as photocathode in water splitting system. In order to distinguish the characteristics of CZTS NSs as photocathode, the PEC performance of CZTS NSs was evaluated compared to planar CZTS film. The thickness of the film was determined to be about 1μm, ensuring that the volume per unit area of the two contrastive samples is approximately the same (Supporting Information, Fig. S6). The PEC performances were tested using a three-electrode cell, where the CZTS NSs or film covered fluorine-doped tin oxide (FTO) substrate as the working electrode, a platinum foil as the counter electrode, and Ag/AgCl as the reference electrode. Fig. 4 displays the current density-potential plots for CZTS NSs and film in the dark and under AM 1.5 illumination. The cathodic photocurrents indicate that CZTS NSs and film was p-type semiconductor. As shown in Figure 4, CZTS NSs photocathode presents considerably higher photocurrent density than that of CZTS film. A photocurrent density of about -1.2 mA/cm^2 at 0 V versus RHE (when stabilized) was obtained for NSs photocathode, which is about 2.4 times that of the CZTS film (-0.5 mA/cm^2). To our best knowledge, this is the highest value ever reported for a CZTS photocathode without further cocatalyst and surface modification.[9,11,14] Moreover, it is worth noticing that the onset potentials of photocurrent for NSs and film are +0.48 V and +0.47 V versus RHE, respectively. The stability test of CZTS photocathodes were performed at a potential of 0 V versus RHE. The current-time curve shows that 60% of the initial photocurrent of NSs can conserve and is still higher than that of film after 3.5 h of testing, suggesting the excellent PEC stability under hydrogen evolution condition. However, the planar film seems more stable than NSs under illumination, which may due to the smaller surface exposed to electrolyte in comparative with NSs. The stability discrepancy observed in CZTS NSs and film photocathodes was still under detailed investigation.

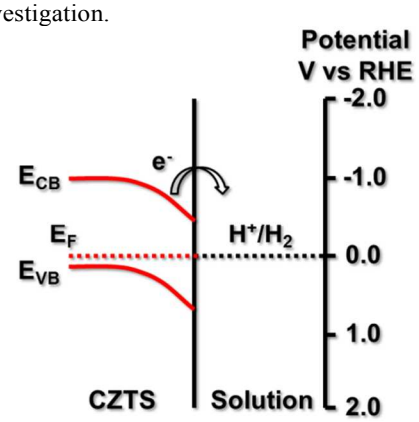

Fig. 5 Energy band position of CZTS with respect to water redox potential determined by Mott-Schottky analysis.

To identify the band edge position of CZTS NSs with respect to water redox potential, the Mott-Schottky (M-S) analysis was conducted. A typical M-S plot of $1/C^2$ versus RHE potential is presented in Fig. S7. The negative slope of M-S plot indicates that CZTS NSs are indeed p-type semiconductor. By intercepting the M-S curve with the *x*-axis, a flat band potential of 0.74 V versus RHE is obtained. From the slope of M-S plot, the acceptor concentration of CZTS NSs, N_A, is calculated as 3.68×10^{20} cm^{-3}. This value is much higher than that of the reported nanocrystalline CZTS film ($1\sim3\times10^{18}$ cm^{-3}),[33] thus favorable for charge separation and transportation. Fig. 5 shows the energy band diagram of CZTS NSs with regard to water redox potentials based on the flat band potential measured

above. Here Fermi level was estimated 0.04 eV over the valence band for CZTS.[33] As seen, the bottom of the conduction band of CZTS NSs is located -0.73 V versus RHE, indicating CZTS NSs can effectively drive the hydrogen-generation reaction.

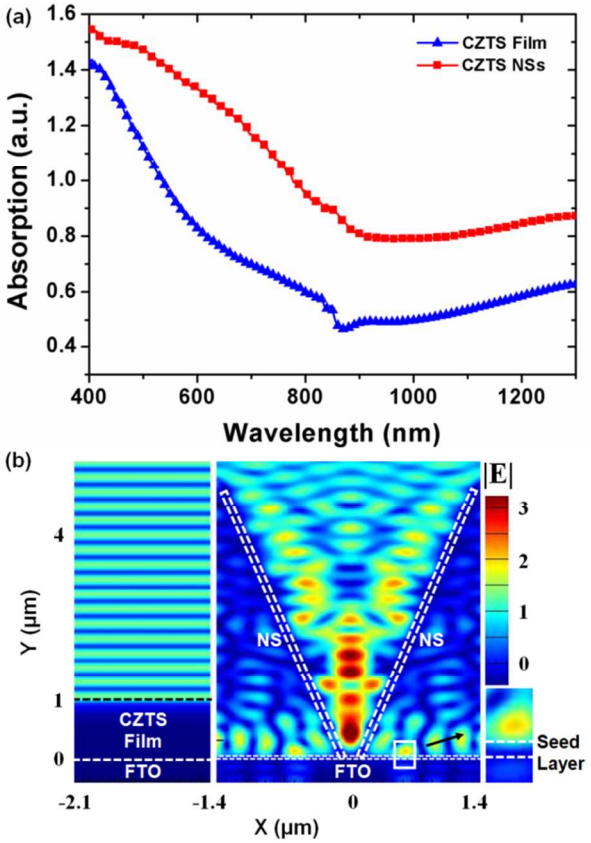

Fig. 6 Optical absorption measurement and simulation of CZTS NSAs and film. (a) UV-vis optical absorption spectra of CZTS NSAs and film. (b) Simulative electric field distributions for CZTS film and NS under TE-polarized illumination at 500nm.

In order to figure out the origin of PEC difference in CZTS NSAs and film, the absorption property and carrier dynamics were characterized. Fig. 6a shows the absorption spectra of NSAs and film, absorption values increase gradually from ~850 nm for both film and NSAs, then reach their peaks at ~450 nm. Obviously, the NSAs show much better light absorption than the planar film. To further investigate the physical mechanism of the enhanced absorption for NSAs, finite difference time domain (FDTD) simulations were performed. Fig. 6b is the electric fields of film and NSAs under TE-polarized illumination at 500 nm. For film, the electric fields distribute mainly over the film, suggesting a dramatic surface reflection effect at the semiconductor/air (or water) interface. On the contrary, in the case of NSAs, the strongest electric fields appear within the cavity surrounded by the NSs, which indicates the incident light is restricted in the sample. The experimental reflectance spectra of the CZTS film and NSAs structure also verify the above results (Supporting Information, Fig. S8). Hence, the absorption enhancement of the NSAs was attributed to their excellent anti-reflection and light trapping effect, which is certainly highly preferable for solar water splitting.

EIS was further conducted to characterize the carrier dynamics in the photocathodes. It is well known that the carrier lifetime (τ_r) in electrodes can be estimated from the plots, using the equation,[34-36]

$$\tau_r = 1/(2\pi f_{max}) \quad (1)$$

As shown in Bode phase plots under illumination of AM 1.5 (Fig. 7), the f_{max} values for CZTS NSAs and film are 3.16 and 7.94 Hz, respectively. Therefore, the carrier lifetimes are calculated to be 50 and 20 ms for NSAs and film, respectively. The longer lifetime for NSAs indicates a lower carrier recombination loss in NSs. As a result, more electrons can transfer to the electrolyte to generate hydrogen, leading to the considerable improvement of photocurrent.

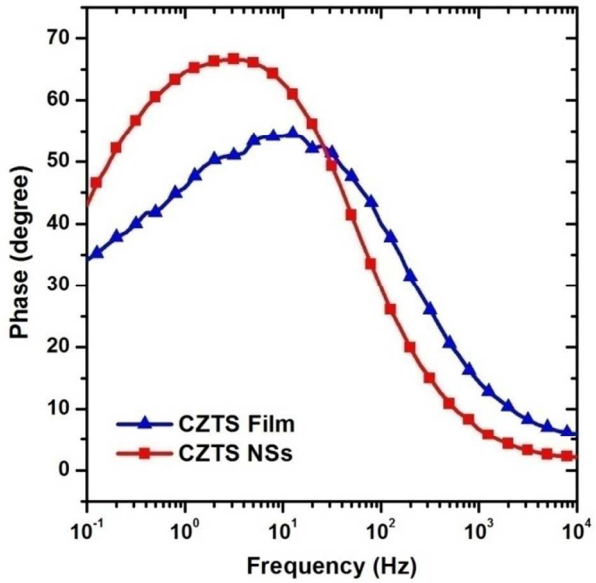

Fig. 7 Bode phase plots of CZTS NSAs and film under the illumination of AM 1.5.

According to the above analysis, the obvious enhancement of photoelectric activity of NSAs in comparative to planar film could be ascribed to the following three aspects. First, the single crystalline NSs with high conductivity provide direct carrier transport pathways for photo-generated carriers, thus effectively reduce resistance and increase the carrier collection efficiency. Second, the NSs possess large surface area contacting with electrolyte, which enables charge separation in the lateral direction, hence significantly reduces the minus diffusion length, depresses carrier recombination and prolongs their lifetime. Third, the specific NS morphology effectively increases the optical length inside the NSAs and reduces reflections, resulting in a considerable improvement of the light absorption.

4. Conclusions

We demonstrated a scalable route for the fabrication of single crystalline CZTS NSAs on transparent conductive substrate using CuS NSAs as sacrificial templates. The CZTS NSAs can significantly enhance charge transportation, improve light absorption, reduce carrier recombination, and thus achieve an ideal photocurrent for hydrogen generation. The unique single crystalline CZTS NSAs pave a new avenue for efficient PEC

water splitting. The further performance enhancement can be anticipated by introducing protection layers as well as hydrogen evolution catalyst, such as Pt or MoS_2.

Acknowledgements

This work was supported by The National Basic Research Program of China (2014CB931703), the Natural Science Foundation of China (No. 21203099, 51171127, 51102176 and 51271129), the Natural Science Foundation of Tianjin City (No. 12JCZDJC29600 and 13JCYBJC36800), and Open Research Fund of State Key Laboratory of Luminescent Materials and Devices (2014-skllmd-05).

Notes and references

1. M. Gräetzel, *Nature,* 2001, **414**, 338-344.
2. N. S. Lewis, D. G. Nocera, *Proc. Natl. Acad. Sci. USA,*2006, **103**, 15729-15735.
3. C. G. Morales-Guio, S. D. Tilley, H. Vrubel, M. Gräetzel, X. Hu, *Nature Commun.,* 2014, **5**, 3059.
4. A. Paracchino, V. Laporte, K. Sivula, M. Gräetzel, E. Thimsen, *Nat. Mater.,* 2011, **10**, 456-461.
5. Z. Li, W. Luo, M. Zhang, J. Feng, Z. Zou, *Energy Environ. Sci.,* 2013, **6**, 347-370.
6. A. F. K. Honda, *Nature,* 1972, **238**, 37-38.
7. M. G. Walter, E. L. Warren, J. R. McKone, S. W. Boettcher, Q. Mi, E. A. Santori, N. S. Lewis, *Chem. Rev.,* 2010, **110**, 6446-6473.
8. K. Sivula, F. Le Formal, M. Gräetzel, *ChemSusChem,* 2011, **4**, 432-449.
9. C. X. Kronawitter, L. Vayssieres, S. Shen, L. Guo, D. A. Wheeler, J. Z. Zhang, B. R. Antoun, S. S. Mao, *Energy Environ. Sci.,* 2011, **4**, 3889-3899.
10. H. Katagiri, K. Jimbo, W. S. Maw, K. Oishi, M. Yamazaki, H. Araki, A. Takeuchi, *Thin Solid Films,* 2009, **517**, 2455-2460.
11. K. Jimbo, R. Kimura, T. Kamimura, S. Yamada, W. S. Maw, H. Araki, K. Oishi, H. Katagiri, *Thin Solid Films,* 2007, **515**, 5997-5999.
12. M. A. Green, *Solar Cells: Operating Principles, Technology and System Applications*, Prentice-Hall, 1981.
13. D. Yokoyama, T. Minegishi, K. Jimbo, T. Hisatomi, G. Ma, M. Katayama, J. Kubota, H. Katagiri, K. Domen, *Appl. Phys. Express,* 2010, **3**, 101202.
14. X. Wen, W. Luo, Z. Zou, *J. Mater. Chem. A,* 2013, **1**, 15479-15485.
15. L. Rovelli, S. D. Tilley, K. Sivula, *ACS Appl. Mater.Interfaces,* 2013, **5**, 8018-8024.
16. E. Ha, L.Y. S. Lee,J. Wang, F. Li, K.-Y. Wong, S. C. E. Tsang, *Adv. Mater.,* 2014, **26**, 3496.
17. G. Ma, T. Minegishi, D. Yokoyama, J. Kubota, K. Domen, *Chem. Phys. Lett.,* 2011, **501**, 619-622.
18. Z. Guan, W. Luo, Z. Zou, *CrystEngComm,* 2014, **16**, 2929-2936.
19. D. A. R. Barkhouse, O. Gunawan, T. Gokmen, T. K. Todorov, D. B. Mitzi, *Prog. Photovoltaics,* 2012, **20**, 6-11.
20. B. Shin, O. Gunawan, Y. Zhu, N. A. Bojarczuk, S. J. Chey, S. Guha, *Prog. Photovoltaics, 2013*, **21**, 72-76.
21. T. K. Todorov, J. Tang, S. Bag, O. Gunawan, T. Gokmen, Y. Zhu, D. B. Mitzi, *Adv. Energy Mater.,* 2013, **3,** 34-38.
22. W. Wang, M. T. Winkler, O. Gunawan, T. Gokmen, T. K. Todorov, Y. Zhu, D. B. Mitzi, *Adv. Energy Mater.,* 2014, **4**.
23. L. Shi, C. Pei, Y. Xu, Q. Li, *J. Am. Chem. Soc.,* 2011, **133**, 10328-10331.
24. Y. Lei, H. Jia, W. He, Y. Zhang, L. Mi, H. Hou, G. Zhu, Z. Zheng, *J. Am. Chem. Soc.,* 2012, **134**, 17392-17395.
25. J. Yu, J. Fan, K. Lv, *Nanoscale,* 2010, **2**, 2144-2149.
26. Y. Qiu, W. Chen, S. Yang, *J. Mater. Chem.,* 2010, **20**, 1001-1006.
27. W. Ki, H. W. Hillhouse, *Adv. Energy Mater.,* 2011, **1**, 732-735.
28. G. G. S. Levcenko, M. Guc, A. Nateprov,*J. Phys. Sci.,* 2009, **8**, 173-177.
29. W. Bi, M. Zhou, Z. Ma, H. Zhang, J. Yu, Y. Xie, *Chem. Commun.,* 2012, **48**, 9162-9164.
30. Q. Guo, S. J. Kim, M. Kar, W. N. Shafarman, R. W. Birkmire, E. A. Stach, R. Agrawal, H. W. Hillhouse, *Nano Lett.,* 2008, **8**, 2982-2987.
31. A. Singh,H. Geaney,F. Laffir, K. M. Ryan, *J. Am. Chem. Soc.,* 2012, **134**, 2910-2913.
32. X. Lu, Z. Zhuang, Q. Peng, Y. Li, *Chem. Commun.,* 2011, **47**, 3141-3143.
33. S. Huang, W. Luo, Z. Zou, *J. Phys. D: Appl. Phys.,* 2013, **46**, 235108.
34. R. Kern, R. Sastrawan, J. Ferber, R. Stangl, J. Luther, *Electrochim. Acta,* 2002, **47**, 4213-4225.
35. Y. H. Jang, X. Xin, M. Byun, Y. J. Jang, Z. Lin, D. H. Kim, *Nano Lett.,* 2012, **12**, 479-485.
36. C. Cheng, S. K. Karuturi, L. Liu, J. Liu, H. Li, L. T. Su, A. I. Y. Tok, H. J. Fan, *Small,* 2012, **8**, 37-42.

†These authors contribute equally to this work.
*E-mail: lingt04@tju.edu.cn, xwdu@tju.edu.cn

